Soft Matter

Accepted Manuscript

ROYAL SOCIETY OF CHEMISTRY

www.rsc.org/softmatter

Diffusing Colloidal Probes of Cell Surfaces

*Gregg A. Duncan[1], D. Howard Fairbrother[2], Michael A. Bevan[1]**
[1]Chemical & Biomolecular Eng., [2]Chemistry, Johns Hopkins Univ., Baltimore, MD 21218

Abstract

Measurements and analyses are reported to quantify dynamic and equilibrium interactions between colloidal particles and live cell surfaces using dark field video microscopy. Two-dimensional trajectories of micron-sized polyethylene glycol (PEG)-coated silica colloids relative to adherent epithelial breast cancer cell perimeters are determined allowing measurement of position dependent diffusivities and interaction potentials. PEG was chosen as the material system of interest to assess non-specific interactions with cell surfaces and establishes a basis for investigation of specific interactions in future studies. Analysis of measured potential energies on cell surfaces reveals the spatial dependence in cell topography. With the measured cell topography and models for particle-cell surface hydrodynamic interactions, excellent agreement is obtained between theoretical and measured colloidal transport on cell surfaces. Quantitative analyses of association lifetimes showed that PEG coatings act to stabilize colloids above the cell surface through net repulsive, steric interactions. Our results demonstrate a self-consistent analysis of diffusing colloidal probe interactions due to conservative and non-conservative forces to characterize biophysical cell surface properties.

Introduction

Our understanding of living cells has greatly benefited from the use of colloidal particles as probes to measure the dynamics of biological processes. For example, biomolecules within the lipid bilayers of cells can be directly tagged with colloidal markers to measure diffusion rates and association kinetics.[1] Transport of endogenous (e.g. lipid vesicles, granules) and synthetic colloidal probes in the cytoplasm has been used to study microrheological properties of cells.[2-6] In addition, the diffusion and fate of colloids interacting with cells has been extensively studied to understand cell entry and transport mechanisms (e.g. endocytosis, phagocytosis, active transport) important to drug delivery.[7-11] While colloidal probes have been used extensively to study intracellular properties of living cells, there have been fewer studies where colloidal probes are used to measure extracellular properties such as ligand-receptor mediated binding, membrane associated biomolecules, and cell topography which have importance to many facets of biology and medicine.

Scanning probe techniques such as atomic force microscopy and optical tweezers have been used to make direct, quantitative measurements of cell morphology and binding at cell surfaces.[12, 13] However by requiring application of external force, the sensitivity and resolution of these techniques is limited to the retraction or trapping force applied by these instruments. Diffusing colloidal probe microscopy (DCPM) techniques allow for sensitive, kT-scale measurement of interfacial interactions, as external manipulation is not necessary. DCPM can be applied using a variety of imaging modalities where inverse analyses of measured particle trajectories are related to net surface potentials and hydrodynamic interactions.[14] Total internal reflection video microscopy can be used to track colloidal probes in three dimensions (3D) with high spatial resolution and is best suited to measuring particle-wall interactions.[15-22] Optical

* To whom correspondence should be addressed. email: mabevan@jhu.edu

video microscopy (OVM) has been used to track colloidal probes in two dimensions (2D) to measure particle-particle interactions[23-26] and topography of chemically patterned surfaces.[27] Using these approaches, we have studied a range of biological systems including polysaccharides,[17, 23] proteins,[16, 19, 20] and supported lipid bilayers.[18, 24] In order to apply DCPM to interrogate cell surfaces, the dynamics of colloidal probes as they diffuse near the surface of live cells must be quantitatively measured over long observation times to collect sufficient statistics. At these time scales, live cells may also migrate and consequently, the position of cells over time also needs to be determined. To our knowledge, algorithms capable of tracking both colloids and cells simultaneously have not been developed in prior studies.

Here, we describe how DCPM can be applied to measure colloidal interactions with the surface of live cells. We introduce a new imaging technique for DCPM using dark field video microscopy (DFVM) to simultaneously image colloidal particles and live cells in real time. Cell surfaces are interrogated using micron-sized colloidal probes above the size limit for passive cell uptake. We have developed image analysis algorithms capable of identifying both cells and colloids, tracking their positions, and measuring the distance between colloids and cell perimeters over time. A number of challenges arise in developing tracking algorithms for this purpose due to the simultaneous motion of particles and cells and the presence of endogenous colloidal materials within the cells that can cause significant errors in these measurements. We have carefully considered each of these issues and designed an algorithm capable of distinguishing colloidal probes from cells and accurately tracking their motion with respect to each other. Polyethylene glycol (PEG) modified colloidal probes were chosen as a model system routinely used in biomedical applications to validate our technique. Equilibrium and hydrodynamic interactions both off and on the cell surface are quantified based on statistical mechanical and dynamic analyses to yield ensemble average potential energies, mean squared displacements, and association lifetimes. Our experimental and analytical approach provides a basis for the study of macromolecule mediated colloid-cell surface interactions important to basic biological functions and biomedical applications.

Materials & Methods

The material system consists of SiO_2 colloids, nominal diameter of 1 and 1.6 μm, with adsorbed PEG layers as described in previous work.[17, 28] Briefly, PEG-PPO-PEG triblock copolymer (F108 Pluronic) was physisorbed on hydrophobically-modified SiO_2 colloids to create ~11 nm PEG brush layers on their surface. The F108-coated particles were sufficiently washed with phosphate-buffered saline (PBS) to ensure free, unabsorbed F108 is completely removed to avoid potential depletion-mediated surface attraction.[29] We have also confirmed in prior studies washing of F108-coated particles does not cause desorption of the F108 from the particle surface.[16, 17, 19, 20, 29] Hydrophobic glass cover slips were made by spin coating polystyrene onto glass cover slips. Based on prior work, we estimate the surface roughness of polystyrene coated glass cover slips to be ~5 nm[30] and have found it does not effect measurements of macromolecular layer thickness.[16, 17, 19, 20, 29] MDA-MB-231 epithelial breast cancer cells in complete media (10% (v/v) fetal bovine serum (FBS) in Dulbecco's modified eagle medium) were seeded onto a small 18mm x 18mm hydrophobic glass cover slip, and allowed to adhere overnight. To create batch cells for experiments, an O-ring was adhered to a hydrophobic glass cover slip and 100 μL of 5 mg/mL bovine serum albumin (BSA) in PBS was absorbed for ~6 hours. This BSA adsorption step was done to prevent non-specific adhesion of colloidal particles to the cover slip. Excess, unadsorbed BSA was rinsed out and 100μL of PEG-coated silica

particles in complete media were added to the O-ring before irradiated with UV for 30 min to sterilize the sample. The O-ring was then removed and the smaller cell-seeded glass cover slip was placed on top of the large slide with particles. The entire assembly was then sealed with nail polish. The cover slip with BSA adsorbed is roughly 1 mm away from the cell-seeded coverslip after assembly and should not affect the measurements.

Using DFVM, colloidal particles and live cells were imaged simultaneously. The samples were inverted for particles to sediment onto the surface with adherent cells and placed on the microscope stage with an attached temperature controller kept at 37ºC for the duration of the experiment. Experiments were performed using an inverted optical microscope with a dark field condenser and a 40x objective. Images are collected with a 12-bit CCD camera with an image area, A_i = 336 pixels x 256 pixels = 203 μm x 155 μm and a 1 Hz frame rate for a total of 1800 frames (30 min duration). The number density of particles in each experiment was kept below an area fraction of 0.02 (~100 particles/image window) in order to limit particle-particle interactions, but above >0.005 (~25 particles/ image window) in order to collect sufficient statistics for equilibrium analysis of particle-cell surface interactions. While achieving equilibrium sampling of all coordinates on the entire surface is prohibitive at these low number densities without long observation times ($t \approx 10^4$ mins), we are able collect sufficient statistics over smaller regions of interest (~500 μm^2/cell x ~8 cells/image window $\approx$ 4000 μm^2 total) at these low number densities in a shorter observation time ($t \approx 25$ mins).[22, 31]

To conduct these studies, custom MATLAB routines were developed and optimized to allow for accurate measurement of colloidal diffusion in the presence of adherent cells. The steps taken in the algorithm are summarized in Figure 1. The location of each cell surface boundary coordinates are defined from DFVM images using the MATLAB Image Processing Toolbox™. Particle centers were tracked using previously reported MATLAB routines.[32] The primary challenges in the image analysis are simultaneously distinguishing particle centers and cell perimeters. Since the intensity of scattering from silica particles and live cells is relatively similar under dark field illumination, additional analysis is required since differentiating between particle and cell scattering based on intensity alone is not possible.

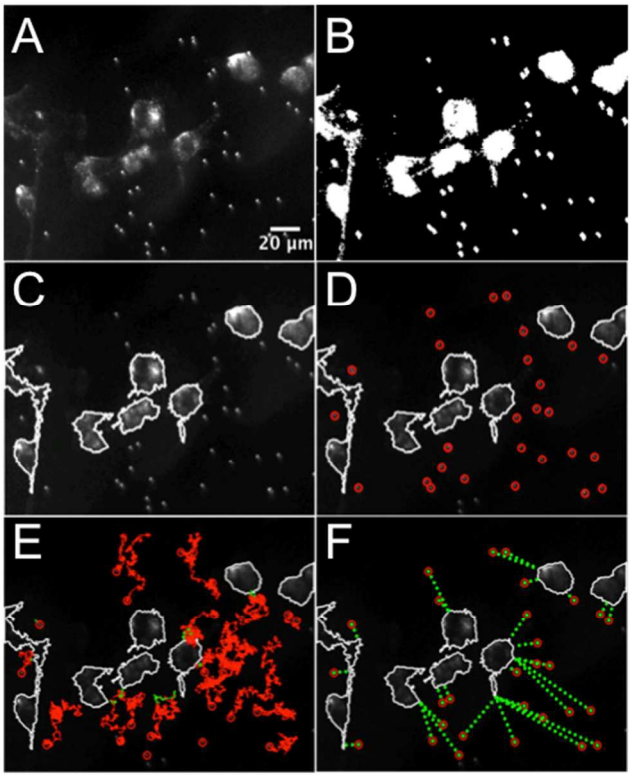

Figure 1. Image analysis of dark field video microscopy (DFVM) experiments of PEG-coated SiO_2 colloids interacting with MDA231 cells. (A) The original image from DFVM experiments showing particles and cells. (B) Binary image produced from thresholding original image in (A). (C) Cell boundaries (white lines) determined from binary image in (B). (D) Particle centers (red circles) determined based on brightness and origin of trajectories outside of determined cell boundaries in (C). (E) Particle trajectories off the cell (red solid lines) and on the cell (green solid lines). (F) Measured particle-cell surface radial distance, r, (dashed green line).

The tracking algorithm first makes a raw dark field image (Fig. 1A) into a binary image via thresholding (Fig. 1B) that shows both cells and colloidal particles. Cells are identified using a size criteria as cells were typically 10-20 times larger than the silica particles studied in this work. Objects from the thresholded image with areas greater than 500 μm^2 were labeled as cells and boundary points were determined (Fig. 1C). Particle centers (Fig. 1D) are differentiated from intracellular components using the condition that particles for analysis must have a trajectory

(solid red lines in Fig. 1E) that begins outside of the cell boundaries. While this eliminates particles starting within the boundaries, this ensures that all trajectories included for analysis are colloids and not scattering points within the cell. In addition to constructing colloidal trajectories, the distance between the particle center and each boundary coordinate, r, is measured and the nearest boundary point is recorded as the particle distance from the cell (Fig. 1F).

To accurately measure colloidal interactions and dynamics at the cell surfaces, the particle-cell boundaries distance must be resolved accurately in the presence of 2D translation of both particles and live cells. Fig. 2 shows ensemble average particle-cell distribution functions, $p(r)$, which illustrates how choice of analytical parameters impacts the accuracy of measured r. In Fig. 2A, the cell boundaries were updated in each frame (t_{update} = 1 s) and the distributions show no sampling at $0<r<3$µm when the particle approaches the cell surface. This is an artifact of the image analysis scheme as the particle becomes incorporated into the newly defined cell boundary (shown in accompanying images in Fig. 2A). To mitigate this effect, t_{update} was increased to the time scale of cell migration. Based on the average lateral migration rate of MDA231 cells (≈1 µm/min),[33] t_{update} was set to 60 s and the resulting particle-cell surface radial distribution is shown in Fig 2B. In this distribution, sampling is recovered in the range $0<r<3$µm as the cell boundary artifact is eliminated. The accompanying images in Fig. 2B also show that the boundary does not artificially incorporate the particle into the cell boundary as it approaches the cell surface.

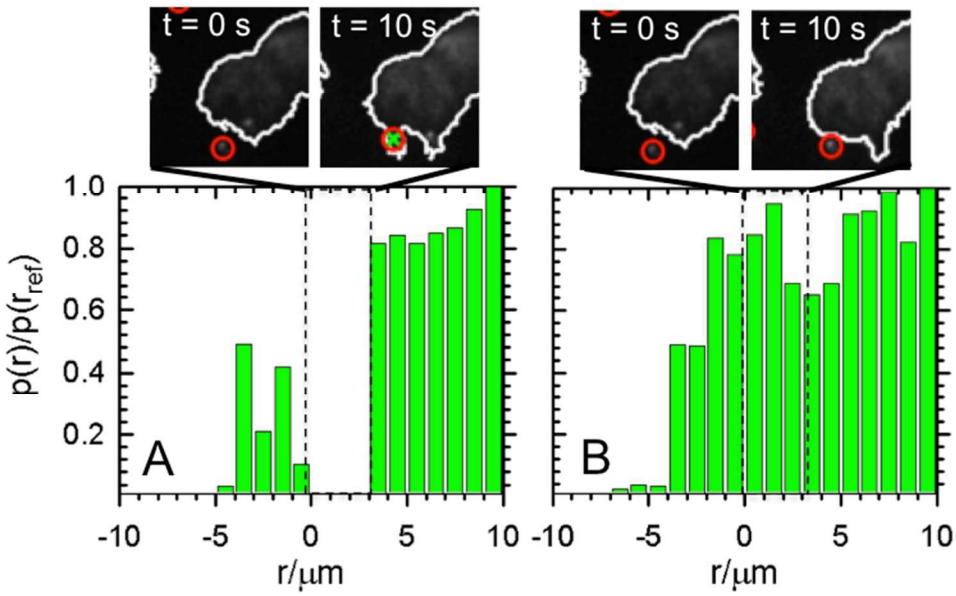

Figure 2. Ensemble average particle-cell surface distribution function, $p(r)$, with (A) continuously updated cell boundaries and (B) boundaries updated every 60 s of 1.6 µm PEG-coated SiO_2 colloids interacting with MDA231 cells. Insets show example images of determined cell boundaries and particle position with respect to the cell boundaries. Boundaries are shown as solid white lines. Particle centers are marked with red circles and when within cell boundaries, additionally marked with green x's.

Theory

Using an equilibrium statistical mechanical analysis, the measured radial distribution of colloids with respect to the cell perimeter can be related to quasi-2D colloid-cell interactions. Based on the distributions of particle-cell radial distance, the particle-cell potential of mean force, $W(r)$, is calculated via a Boltzmann inversion as,[34, 35]

$$W(r)/kT = -\ln[p(r)/p(r_{ref})] \quad (1)$$

where k is Boltzmann's constant, T is temperature, and r_{ref} is a chosen reference r where $W(r_{\mathrm{ref}})=0$. In the present case, we let the potential equal zero as r goes to infinity (where particles and cells do not interact). By assuming the potential of mean force is determined by a gravitational potential energy landscape without many-particle packing effects, $W(r)$ can be related to the cell surface topography, $h(r)$, as,[27]

$$h(r) = W(r)/mg = W(r)/[(4\pi/3)(\rho_p - \rho_w)a^3 g] \quad (2)$$

where m is the particle buoyant mass, g is the acceleration due to gravity, a is the particle radius, ρ_{p} is the particle density, and ρ_{w} is the fluid density.

In addition to equilibrium analyses of particle trajectories, measured ensemble average colloidal dynamics off and on the cell surface were interpreted considering the role of particle-surface hydrodynamic interactions. Hydrodynamic interactions with the underlying substrate and cell surface will slow down the lateral motion of the particle from its predicted Stokes-Einstein diffusivity, $D_0=kT/6\pi\mu a$ where μ is the fluid viscosity. Fig. 3 depicts the most relevant length scales to diffusion of colloidal particles near an interface with adherent cells. Hydrodynamic interactions will depend on the particles relative height above the underlying substrate or cell surface, depending on r, defined here as,

$$\Delta = z - h(r) \quad (3)$$

where z is the absolute height of the particle center above the underlying substrate. On the cell surface, Δ is the height of the particle center above the cell surface and off the cell surface, this height reduces to $\Delta=z$. Hydrodynamic effects can be accounted for with a separation dependent diffusion coefficient as,

$$D(\Delta) = D_0 f_{\parallel}(\Delta) \quad (4)$$

where $f_{||}$ is a rational fit to the exact solution of Brenner's hydrodynamic correction factor defined as,[19, 23, 35]

$$f_{\parallel} = \frac{368\phi^3 + 559\phi^2 + 81\phi}{368\phi^3 + 779\phi^2 + 250\phi^3} \quad (5)$$

where $\phi=(\Delta-(a+\delta_p+\delta_s)/(a+\delta_p+\delta_s)$, δ_p and δ_s are the macromolecular layer thickness on the particle and surface, respectively. The thickness of the PEG coating on the colloids, δ_p=11 nm, is estimated based on prior measurements[17] and the macromolecular layer thickness on the substrate and cell surfaces, δ_s, is left as the only adjustable parameter in the model. This estimate of macromolecular layer thicknesses assumes that the layers do not interpenetrate.

A theoretical net particle-surface interaction potential is defined as the superposition of contributing potentials, $u(z)=u_G(z)+u_V(z)+u_S(z)$, which includes gravitational (G), van der Waals (V), and steric interactions (S). The net gravitational potential depends on the buoyant weight of the particle and is defined as, $u_G(z) = mgz = (4/3)\pi a^3(\rho_p-\rho_w)z$. The net van der Waals interactions can be predicted using the Derjaugin approximation with Lifshitz theory. For convenience, we use a power-law expression defined as, $u_V(z) = -aA(l)z^{-p}$, where A is an effective Hamaker constant dependent on particle, cell, and substrate composition and p = 2.15 is the noninteger power for retarded van der Waals interactions.[21]

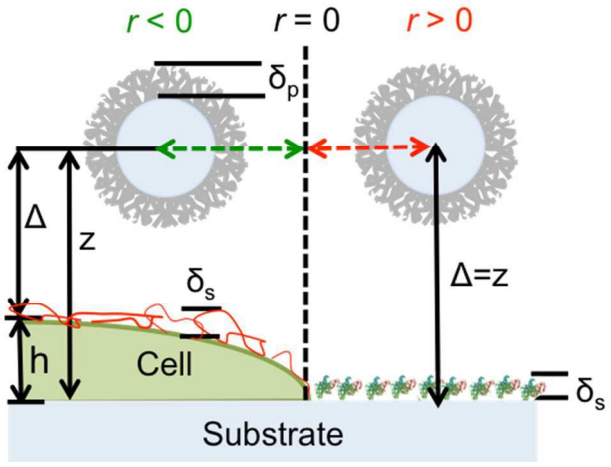

Figure 3. Schematic showing relevant length scales for colloidal diffusion near an interface with adherent cells. The schematic shows a colloidal particle with PEG layer thickness, δ_p, at a radial position $r < 0$, diffusing on a cell of height h and extracellular coat (i.e. glycocalyx) thickness, δ_s. The particle has an absolute height, z, above the substrate and is at a height $\Delta=z-h$ above the cell. It also depicts a colloidal particle at a radial position $r > 0$, diffusing above the substrate with serum protein coating, δ_s at a height $\Delta=z$.

The value of constants defined for each contributing potential are dependent on the particles' position either on the background substrate or the cell surface. For the particle-background substrate interactions, A=2.1 kT nm$^{1.15}$ as determined previously for van der Waals interactions between a particle and surface composed of silica.[21] For the particle-cell surface interactions, A=3.1 kT nm$^{1.15}$ as determined from a fit to Lifshitz theory predictions used in prior work for supported lipid bilayers.[18] Steric interactions due to repulsion generated between macromolecular layers at adjacent interfaces can be estimated using Milner's brush theory with asymmetric macromolecular layer properties accounted for using the bisection rule, described in detail elsewhere.[17, 20] For simplicity, we use a short-range exponential that effectively captures

these effects defined as, $u_S(z)=10kT[\exp[-\kappa_S(z-a-\delta_{HW})]]$ where $\kappa_S=3$ nm^{-1} is an inverse decay length and δ_{HW} is the layer thickness at maximum compression approximated as $\delta_{HW}=(\delta_p+\delta_s)-4.1\kappa_S^{-1}$.[24]

The distribution of heights sampled by the particles above the underlying substrate or cell surface, $p(\Delta)$, can be calculated with Boltzmann's equation as,

$$p(\Delta) = \exp(-u(\Delta)/kT) \tag{6}$$

Prediction of the average lateral diffusion coefficient at a height h above the substrate/cell surface, $\langle D_h \rangle$, that takes into account the distribution of heights sampled by the particle is given by,[19, 23]

$$\left\langle D_h \right\rangle = \frac{\int_a^\infty D(\Delta)p(\Delta)d\Delta}{\int_a^\infty p(\Delta)d\Delta} \tag{7}$$

On the cell surface, particles will also experience migration down an incline due to local changes in cell surface topography and the sedimentation velocity, v_s, can be calculated as,[36]

$$v_s = 2a^2\Delta\rho g \tan\theta / 9\mu \tag{8}$$

where θ is the local incline angle. The average local incline due to cell surface topography, $\langle\theta\rangle$, can be calculated as

$$\left\langle \theta \right\rangle = \sum_{r=-0.5\mu m}^{-10\mu m} \tan^{-1}[\Delta h(r)/\Delta r]p(r) \tag{9}$$

based on measured $h(r)$ and weighted using measured $p(r)$. An effective diffusion coefficient, D_{eff}, that accounts for both diffusion and migration on the cell surface can then be determined as,[37]

$$D_{eff} = \left\langle D_h \right\rangle + v_s^2\tau_s/4 \tag{10}$$

where $\tau_s = L_s^2/\langle D_h \rangle$, is the characteristic time to change direction due to local surface elevation changes with length scale, L_s.

The association lifetime of a colloidal particle to a surface, t_a, is dependent on the characteristic time scale of diffusion, τ_a, and colloid-surface attractive energy well, u_{min}, as approximated by, [17, 19]

$$t_a \approx \tau_a \exp(|u_{min}|/kT) \tag{10}$$

where $\tau_a=L_a/\langle D_h \rangle$, L_a is set to be the pixel size of DFVM images and $\exp(|u_{min}|/kT)$ is the probability a particle will escape an attractive energy well assuming a Boltzmann distribution of

thermal energies and reduces to τ_a in the limit of no net colloid-surface attraction. Equation 10 can be rearranged to relate t_a to u_{min} directly as

$$\ln(t_a / \tau_a) \approx |u_{min}| / kT \quad (11)$$

To determine if colloids were associated to the surface, the position of the particle was monitored for time τ_a = 6 s (6 consecutive images) and if the coordinates in these images had a standard deviation σ_{xy} < 120 nm, the particle was considered associated to the surface. This tolerance was determined from the theoretical diffusion-limited motion of a particle at contact with a surface (as Δ goes to zero) calculated from Eq. (7).

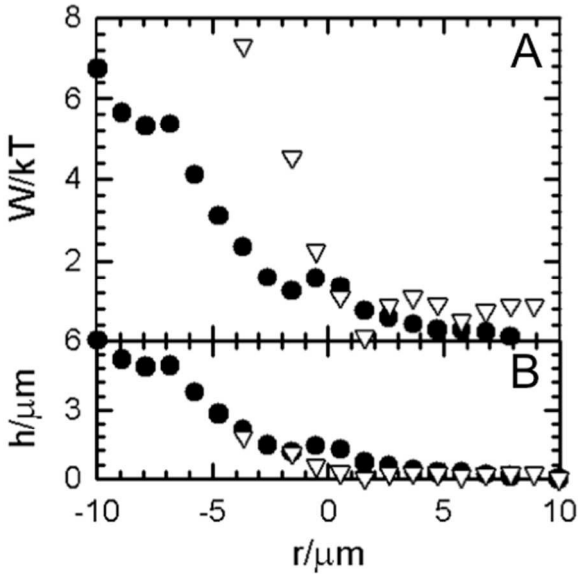

Figure 4. (A) Ensemble average particle-cell surface potentials of mean force, $W(r)$, of 1.6 μm (white triangles) and 1 μm (black circles) PEG-coated SiO_2 colloids interacting with MDA231 cells. (B) Cell height, h, as a function of r calculated with Eq. (2) based on measured $W(r)$.

Results & Discussion

Dynamic and equilibrium surface interactions of PEG-coated colloidal silica with live MDA231 breast cancer cells and the effect of particle size are explored using these analytical tools. In Fig. 4A, $W(r)$ are shown for 1 μm (black circles) and 1.6 μm (white triangles) silica colloids and the average height of the particle, h, as a function of r is shown in Fig. 4B. A much sharper repulsive interaction exists between the particle and cell surface for the 1.6 μm PEG-coated particle compared to the 1 μm PEG-coated particles shown in Fig. 4A. Because both particles have identical surface chemistry, it is unlikely the particles have different net surface interactions with the cell surfaces. We also do not expect size-dependent particle-cell surface interactions, as both sizes are beyond the limit for endocytosis-mediated cell uptake.

It is more likely the difference arises from the change in buoyant weight of the different sized particles. With the typical "hill" shape of cells cultured on 2D substrates, the gravitational

penalty at decreasing r would prevent larger particles from diffusing towards higher elevations towards the cell center. Measured $W(r)$ (Fig. 4A) were interpreted with Eq. (2) and, there is good agreement between measured $h(r)$ profiles for the 1 μm and 1.6 μm PEG-coated silica particles shown in Fig. 4B. We have validated this approach in a prior study where the height profiles measured using DCPM for physically-patterned interfaces were independently confirmed by AFM.[27] While the 1.6 μm particles are limited to sampling heights less than $h \approx 2$ μm, the lighter 1 μm particles are able to make height excursions to positions further on top of the cell up to $h \approx$ 6μm, corresponding to $W \approx 7\ kT$ in each case. It should be noted that these height profiles are calculated based on the potential of mean force, $W(r)$, and the height of the cell as a function of r is averaged spatially and temporally based on particle positions. This height is also an ensemble average over all cells based on statistical sampling of radial positions on their surfaces. With our current methodology, we are unable to resolve the differences in topography between individual cells, effects of cell motility on topography and spatial heterogeneity in extracellular components (e.g. serum proteins, membrane proteins, polysaccharides) on individual cells that would impact these measurements.

To examine colloidal dynamics, trajectories can be subcategorized based on their position with respect to the cell (Fig. 1E) with trajectories drawn as red and green solid lines when off and on the cell surface, respectively. Comparing the dynamics in these subgroups is helpful in interpreting hydrodynamic interactions of particles with cell surfaces. The mean squared

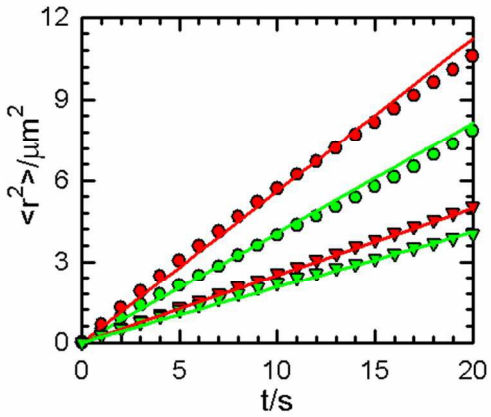

Figure 5. 1D lateral mean squared displacement averaged over the x and y-direction of 1.6 μm (triangles) and 1 μm (circles) PEG-coated silica colloids diffusing off the cell surface (red symbols) and on the cell surface (green symbols). Theoretical fits to MSD are shown as solid lines. Parameters for each fit are summarized in Table 1.

displacement (MSD) calculated for each population of trajectories. Fig. 5 shows 1D MSD averaged over the x and y-direction for 1 μm (circles) and 1.6 μm (triangles) PEG-coated particles both off (red symbols) and on (green symbols) the surface of the cell and each MSD was modeled using Eqs. (7) and (8). The parameters used in these fits are summarized in Table 1.

Table 1. Parameters for theoretical fits to mean squared displacement data (Fig. 5) of PEG-coated SiO_2 colloids on the macromolecule-coated substrate and cell surface. Particle layer thickness (δ_p) used in theoretical fits based on prior measurements.[17]

Particle/Surface	D_{eff}/D_o	L (μm)	⟨θ⟩ (°)	δ_P (nm)	δ_S (nm)
1 μm/substrate	0.69	-	-	11	15
1.6 μm/substrate	0.52	-	-	11	15
1 μm/cell	0.50	1	4.6	11	29
1.6 μm/cell	0.44	1	1.6	11	27

The diffusion rate of 1 μm particles are reduced considerably on the cell surface in comparison to on the background substrate. For the 1.6 μm particles, similar diffusion rates were measured off and on the cell surface. While this difference between particle sizes may not be intuitively expected given their identical surface chemistry, we can conceptually rationalize the role of cell topography on a resulting D_{eff} that accounts for particle sedimentation on an inclined interface. When diffusing on the background substrate, the elevation of the surface can be assumed to be flat and the colloid's position on the surface should not impact its diffusion rate. On the "hill"-shaped cell surface, the particle will migrate with a velocity dependent on their buoyant weight and the local changes in cell surface topography (Eq. 8). Based on measured $h(r)$, lower ⟨θ⟩ were locally experienced by 1.6 μm particles compared to 1 μm particles as they were unable to access higher elevations on the cell which showed steeper gradients in elevation. However given the scaling of the migration component of D_{eff} with particle size ($v_s^2\tau_s \propto a^6$), 1.6 μm particles would experience a far greater migration rate compared to 1 μm particles on the cell surface. Hence, hydrodynamic effects slowing 1 μm particle effective diffusion on the cell surface are more apparent compared to that measured for 1.6 μm particle which migrate more quickly on the cell surface.

We estimated the thickness of macromolecules on the underlying substrate and cell surface based on a theoretical fit to measured effective transport rates that are summarized in Table 1. We predict δ_s=15 nm on the background serum protein-coated substrate for 1 μm and 1.6 μm particles, consistent with prior studies on protein corona formation on nanoparticles with layer thicknesses ranging from 10-20 nm.[38, 39] These predictions of serum protein layer thickness also assume that there is no accumulation of serum proteins on the surface of PEG-coated particles. Based on prior measurements of PEG-bovine serum albumin (BSA) interactions which were net repulsive,[19] we would not expect significant adsorption of serum proteins onto the particle surface.

By accounting for the influence of cell topography and colloidal migration, we estimated thickness of the cell-surface associated macromolecules on the cell surface was ~30 nm for both particle sizes, slightly thicker than that estimated on the underlying substrate. While to our knowledge there are no prior reports of glycocalyx thickness for the MDA-MB-231 cell line studied in this work, an extracellular coating on the order of ~30 nm is consistent with a glycocalyx layer consisting of the extracellular portion of membrane glycoproteins and glycolipids present on the cell surface. The presence of an excreted extracellular matrix (ECM) coating with larger polysaccharide components such as hyaluronic acid is unlikely as prior reports have shown the marked reduction in extracellular coating thickness for cells cultured *in vitro* (20-30 nm) compared to *in vivo* (~520 nm).[40] More specifically for MDA-MB-231 cells, the metastatic potential of this cell line has been linked to differential hyaluronan metabolism, producing ECM coatings with lower MW hyaluronic acid.[41] Based on these findings, an ECM coating of substantial thickness is unlikely to be formed given the *in vitro* culture conditions and cell type used in our study.

There are several limitations of our approach as compared to DCPM measurements employing evanescent wave scattering to track colloids in 3D and extract the particle height directly (compared to DCPM studies using other microscopy methods and geometries).[16-20] In the measurements described here, the height of the particle above the cell or underlying substrate cannot be directly measured and the distribution of heights above the cell surface are modeled using a theoretical net potential (Eq. 6) that has previously been shown to work well for macromolecule coated surfaces and lipid bilayers.[18, 19, 23, 24] The net potential must also be assumed based on our best approximation of net particle-cell surface interactions derived from prior measurements on supported lipid bilayers.[18, 24] There will be large differences in the composition of lipids in the cell membrane, which likely have spatially heterogeneous densities, as compared to a synthetic lipid bilayer coated interface which could impact the net potential. There also are a number of proteins, polysaccharides associated to the surface of live cells, which also likely have spatially heterogeneous densities that could have an impact on these measurements. Our measurements of net particle-cell surface potentials, cell height, and thickness of macromolecules coating the cell surface represent the average of these quantities. However, it is likely for many drug delivery and tissue engineering applications, spatial heterogeneities in biomolecular and biophysical properties will be of less importance compared to the resulting average interaction with cell surfaces. To account for the effects of spatial heterogeneity on the cell surface, this technique in conjuction with dynamic Bayesian inference analyses[15] will be used in future studies to determine combined energy and diffusivity landscapes (*i.e.*, $W(x,y)$, $D(x,y)$) of colloidal probes interacting with cell surfaces.

Another assumption made throughout our analyses is that PEG-coated colloidal particles have purely repulsive interactions with cell surfaces. While PEG conjugation of nanomaterials is often used in biomedical applications to resist adhesion of biomolecules and enhance their stability, there are also reports of significant adsorption of biomolecules to PEG-coated nanomaterials and interfaces, depending on PEG surface density and molecular weight, that could alter their interactions with cells.[42, 43] To assess this in our material system, colloid-cell surface interactions were directly measured through association lifetimes. To determine if colloidal particles have associated to the cell surface, the displacement of the particle can be measured over a characteristic time scale, τ_a, chosen based on the diffusion-limited motion of the particle. In the limit of no net attraction with the cell surface, t_a reduces to the diffusion-limited time τ_a and will increase exponentially with only small increases in net particle-surface attraction. With this measurement, reversible association as well as strong, irreversible association can be detected providing a direct, sensitive measurement of macromolecular interactions at the interface between colloids and cell surfaces.

Figure 6 shows histogram of association lifetimes for 1 μm PEG-coated particles on the substrate and on the cell surface. Each bar has a linear color scale indicating approximate effective attractive energy, $\ln(t_a/\tau_a) \approx |u_{min}|/kT$, also shown in Figure 6. The association lifetime histograms for 1.6 μm PEG-coated particles were very similar to the 1 μm particles (as expected given their identical surface chemistry) and for that reason were not included for discussion. We find that on the substrate roughly 80% of particles associate only short times to the cell surface (Fig. 6A) indicating net repulsive interactions with the underlying substrate. This can be attributed to the presence of ~15 nm serum protein layer preventing non-specific adsorption to the surface (Table 1). On the cell surface (Fig. 6B), roughly 70% of particles associate for short times and show negligible net attraction to the cell surface. A small percentage of particles

associated to the cell surface for longer times with a maximum attraction of ~3 *kT*. This would indicate that PEG-coated particles also have net repulsive interactions with the cell surface likely attributed to a layer of cell-surface associated biomolecules acting as steric barrier to adsorption to the cell.[44-46] While we do detect a small difference in association lifetime profiles between the underlying substrate and the cell, the maximum attraction of 2 and 3 *kT* experienced by the particles on the underlying surface and cell respectively is insufficient to cause significant adsorption to either surface. These results confirm that the PEG coatings were sufficient to prevent nonspecific adsorption to the underlying substrate and cell surfaces.

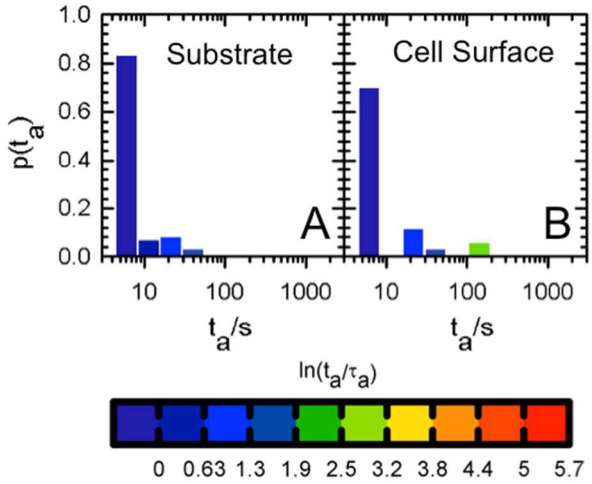

Figure 6. Association lifetime histograms, $p(t_a)$, for 1 μm PEG-coated silica particle on (A) the substrate and (B) cell surfaces. Histograms constructed from particle trajectories outside and within cell boundaries (shown as red, green lines in Figure 1). Each bar has a linear color scale of $\ln(t_a/\tau) \approx |u_{min}|/kT$ shown below.

Conclusions

Measurements of biophysical and macromolecular interactions at the surface of live cells were quantified using diffusing colloidal probes. With the added complexities of intracellular scattering and cell motility, image analysis techniques were developed to accurately measure trajectories of colloidal particles with respect to translating cell perimeters. Measured energy landscapes as a function of particle-cell surface distance and colloidal dynamics on the cell surface show theoretical and experimental agreement when cell topography is taken into consideration. We further confirmed net repulsive interactions exist between PEG-coated particles and cell surfaces through analysis of association lifetimes. PEG-coated colloidal probes show promise for mapping of cell surface topography that could be tailored for characterization of specific cell and tissue types by simply changing particle size. Future studies will interrogate other natural and synthetic biomaterials related to tissue engineering and drug delivery to sensitively measure their interactions with cell surfaces. Ultimately, the results in this work establish a novel method for quantitative measurement of interactions between macromolecule-coated colloidal particles and living cells.

Acknowledgements

We thank Sharon Gerecht (Johns Hopkins) for providing the cells, access to cell culture

facilities, and helpful discussions. We acknowledge financial support by the National Science Foundation (CBET-0834125, CBET-1066254, CHE-1112335, and an IGERT traineeship).

References

1. C. Dietrich, B. Yang, T. Fujiwara, A. Kusumi and K. Jacobson, *Biophysical journal*, 2002, **82**, 274-284.
2. Y. Tseng, T. P. Kole and D. Wirtz, *Biophysical Journal*, 2002, **83**, 3162-3176.
3. a. Lau, B. Hoffman, a. Davies, J. Crocker and T. Lubensky, *Physical Review Letters*, 2003, **91**, 198101.
4. C. Wilhelm, *Physical Review Letters*, 2008, **101**, 028101.
5. M. Duits, Y. Li, S. Vanapalli and F. Mugele, *Physical Review E*, 2009, **79**, 051910.
6. D. Robert, K. Aubertin, J.-C. Bacri and C. Wilhelm, *Physical Review E*, 2012, **85**, 011905.
7. J. Suh, D. Wirtz and J. Hanes, *Proceedings of the National Academy of Sciences of the United States of America*, 2003, **100**, 3878-3882.
8. D. Arcizet, B. Meier, E. Sackmann, J. Rädler and D. Heinrich, *Physical Review Letters*, 2008, **101**, 248103.
9. H. Jin, D. a. Heller, R. Sharma and M. S. Strano, *ACS Nano*, 2009, **3**, 149-158.
10. N. F. Reuel, A. Dupont, O. Thouvenin, D. C. Lamb and M. S. Strano, *ACS nano*, 2012, **6**, 5420-5428.
11. K. Welsher and H. Yang, *Nature nanotechnology*, 2014, **9**, 198-203.
12. D. J. Müller, J. Helenius, D. Alsteens and Y. F. Dufrêne, *Nature Chemical Biology*, 2009, **5**, 383-390.
13. I. Casuso, F. Rico and S. Scheuring, *Journal of Molecular Recognition*, 2011, **24**, 406-413.
14. M. a. Bevan and S. L. Eichmann, *Current Opinion in Colloid and Interface Science*, 2011, **16**, 149-157.
15. D. J. Beltran-Villegas, T. D. Edwards and M. A. Bevan, *Langmuir*, 2013, **29**, 12337-12341.
16. S. L. Eichmann and M. A. Bevan, *Langmuir*, 2010, **26**, 14409-14413.
17. S. L. Eichmann, G. Meric, J. C. Swavola and M. A. Bevan, *Langmuir*, 2013, **29**, 2299-2310.
18. W. N. Everett and M. A. Bevan, *Soft Matter*, 2014, **10**, 332.
19. W. N. Everett, H.-j. Wu, S. G. Anekal, H.-j. Sue and M. A. Bevan, *Biophysical Journal*, 2007, **92**, 1005-1013.
20. J. C. Swavola, T. D. Edwards and M. A. Bevan, *Langmuir*, 2015, **31**, 9076-9085.
21. H.-J. Wu and M. A. Bevan, *Langmuir*, 2005, **21**, 1244-1254.
22. H. J. Wu, W. N. Everett, S. G. Anekal and M. A. Bevan, *Langmuir*, 2006, **22**, 6826-6836.
23. G. A. Duncan and M. A. Bevan, *Langmuir*, 2014, **30**, 15253-15260.
24. W. N. Everett, D. J. Beltran-Villegas and M. A. Bevan, *Langmuir*, 2010, **26**, 18976-18984.
25. J. J. Juarez, J. Q. Cui, B. G. Liu and M. A. Bevan, *Langmuir*, 2011, **27**, 9211-9218.
26. T. D. Edwards and M. a. Bevan, *Langmuir : the ACS journal of surfaces and colloids*, 2012, **28**, 13816-13823.
27. P. Bahukudumbi and M. A. Bevan, *The Journal of Chemical Physics*, 2007, **126**, 244702.

28. A. K. van Helden, J. W. Jansen and A. Vrij, *Journal of Colloid and Interface Science*, 1981, **81**, 354-368.
29. D. J. Beltran-Villegas, T. D. Edwards and M. A. Bevan, *Langmuir*, 2013, **29**, 12337-12341.
30. M. a. Bevan and D. C. Prieve, *Langmuir*, 1999, **15**, 7925-7936.
31. S. H. Behrens and D. G. Grier, *Physical review. E, Statistical, nonlinear, and soft matter physics*, 2001, **64**, 050401.
32. J. C. Crocker and D. G. Grier, *Journal of Colloid and Interface Science*, 1996, **179**, 298-310.
33. D. B. Agus, J. F. Alexander, W. Arap, S. Ashili, J. E. Aslan, R. H. Austin, V. Backman, K. J. Bethel, R. Bonneau, W.-C. Chen, C. Chen-Tanyolac, N. C. Choi, S. A. Curley, M. Dallas, D. Damania, P. C. W. Davies, P. Decuzzi, L. Dickinson, L. Estevez-Salmeron, V. Estrella, M. Ferrari, C. Fischbach, J. Foo, S. I. Fraley, C. Frantz, A. Fuhrmann, P. Gascard, R. A. Gatenby, Y. Geng, S. Gerecht, R. J. Gillies, B. Godin, W. M. Grady, A. Greenfield, C. Hemphill, B. L. Hempstead, A. Hielscher, W. D. Hillis, E. C. Holland, A. Ibrahim-Hashim, T. Jacks, R. H. Johnson, A. Joo, J. E. Katz, L. Kelbauskas, C. Kesselman, M. R. King, K. Konstantopoulos, C. M. Kraning-Rush, P. Kuhn, K. Kung, B. Kwee, J. N. Lakins, G. Lambert, D. Liao, J. D. Licht, J. T. Liphardt, L. Liu, M. C. Lloyd, A. Lyubimova, P. Mallick, J. Marko, O. J. T. McCarty, D. R. Meldrum, F. Michor, S. M. Mumenthaler, V. Nandakumar, T. V. O'Halloran, S. Oh, R. Pasqualini, M. J. Paszek, K. G. Philips, C. S. Poultney, K. Rana, C. A. Reinhart-King, R. Ros, G. L. Semenza, P. Senechal, M. L. Shuler, S. Srinivasan, J. R. Staunton, Y. Stypula, H. Subramanian, T. D. Tlsty, G. W. Tormoen, Y. Tseng, A. van Oudenaarden, S. S. Verbridge, J. C. Wan, V. M. Weaver, J. Widom, C. Will, D. Wirtz, J. Wojtkowiak and P.-H. Wu, *Scientific reports*, 2013, **3**, 1449.
34. B. M. Alexander and D. C. Prieve, *Langmuir*, 1987, **3**, 788-795.
35. E. S. Pagac, R. D. Tilton and D. C. Prieve, *Chemical Engineering Communications*, 1996, **148-150**, 105-122.
36. G. Dunderdale, S. Ebbens, P. Fairclough and J. Howse, *Langmuir*, 2012, **28**, 10997-11006.
37. J. R. Howse, R. A. Jones, A. J. Ryan, T. Gough, R. Vafabakhsh and R. Golestanian, *Physical review letters*, 2007, **99**, 048102.
38. M. P. Monopoli, D. Walczyk, A. Campbell, G. Elia, I. Lynch, F. Baldelli Bombelli and K. A. Dawson, *Journal of the American Chemical Society*, 2011, **133**, 2525-2534.
39. E. Casals, T. Pfaller, A. Duschl, G. J. Oostingh and V. Puntes, *ACS Nano*, 2010, **4**, 3623-3632.
40. D. Chappell, M. Jacob, O. Paul, M. Rehm, U. Welsch, M. Stoeckelhuber, P. Conzen and B. F. Becker, *Circulation research*, 2009, **104**, 1313-1317.
41. L. Udabage, G. R. Brownlee, S. K. Nilsson and T. J. Brown, *Experimental cell research*, 2005, **310**, 205-217.
42. R. Michel, S. Pasche, M. Textor and D. G. Castner, *Langmuir*, 2005, **21**, 12327-12332.
43. M. Malmsten, K. Emoto and J. M. Van Alstine, *Journal of Colloid and Interface Science*, 1998, **202**, 507-517.
44. H. Boehm, T. A. Mundinger, C. H. J. Boehm, V. Hagel, U. Rauch, J. P. Spatz and J. E. Curtis, *Journal*, 2009, **5**, 4331.
45. B. P. Toole, *Nature reviews. Cancer*, 2004, **4**, 528-539.

46. J. Wall, F. Ayoub and P. O'Shea, *Journal of cell science*, 1995, **108 (Pt 7)**, 2673-2682.

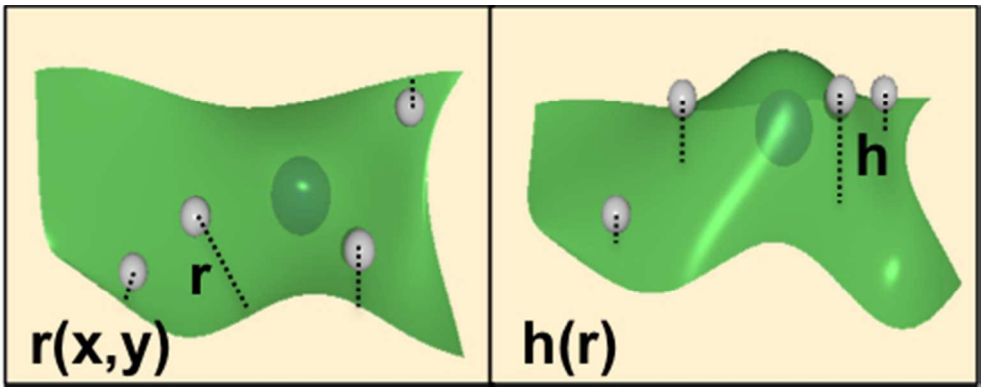

172x67mm (72 x 72 DPI)